Applied Catalysis B: Environmental 99 (2010) 58–65

Contents lists available at ScienceDirect

Applied Catalysis B: Environmental

journal homepage: www.elsevier.com/locate/apcatb

Indoor air purification using heterogeneous photocatalytic oxidation. Part II: Kinetic study

Q.L. Yu*, M.M. Ballari, H.J.H. Brouwers

Department of Architecture, Building and Planning, Eindhoven University of Technology, P.O. Box 513, 5600 MB Eindhoven, The Netherlands

ARTICLE INFO

Article history:
Received 15 March 2010
Received in revised form 26 May 2010
Accepted 28 May 2010
Available online 4 June 2010

Keywords:
Heterogeneous photocatalytic oxidation
Indoor air purification
Nitric oxide
Modified TiO_2
Kinetic model

ABSTRACT

In part I to this article [1], the application of the heterogeneous photocatalytic oxidation (PCO) theory for the indoor air quality improvement was presented. With a modified TiO_2 that can be activated by visible light as the photocatalyst coated on a special wall paper, and one typical indoor air pollutant nitric oxide (NO) as model pollutant, the PCO experiments were performed in indoor air conditions and results show its effectiveness as an indoor air purifying technology.

As the second part of the above mentioned study, this article addresses the kinetics of the photocatalytic oxidation of NO. A kinetic reaction rate model is proposed to describe the PCO of NO under indoor air conditions. The influence of the indoor air conditions such as pollutant concentration, volumetric flow rate of the pollutant, relative humidity, irradiance, dosage of the photocatalyst, and reactor size is considered in this model. As an undesired intermediate product in the process of the PCO of NO nitrogen dioxide (NO_2) is incorporated as well from its influence on the PCO process. The good agreement between the predictions from this model and the experimental results indicates the validity of the proposed kinetic model.

1. Introduction

Heterogeneous photocatalytic oxidation (PCO) has proven to be a successful technology for water or air purification in outdoor conditions and to date the photocatalytic oxidation has been investigated intensively [2]. Also to indoor air quality (IAQ) more and more attention is paid due to the very important role indoor environment plays on human health. Nitrogen oxides (NO and NO_2) and volatile organic compounds (VOCs), as typical inorganic and organic indoor air pollutants, can be emitted from many sources such as cooking, combustion, tobacco smoke, furniture, building materials, even traffic pollutant from outside of building. These indoor pollutants can cause serious health problems like drowsiness, headache, sore throat, and mental fatigue [3]. Therefore, it would be promising if the PCO technology can also be applied to remove these pollutants in order to obtain a better indoor air quality for people's health.

Starting from this idea, the present authors investigated the possibility to improve the indoor air quality with the application of the PCO technology [1]. Visible light was used as the light source for the PCO reaction in order to simulate the real indoor air conditions. A modified TiO_2 was chosen as the photocatalyst since traditional TiO_2 could not be activated by visible light. One special wall paper, used as a cover paper for one novel type of gypsum plasterboard (a sub-research task under the EU research project I-SSB [4]), was chosen as the substrate for the coating of the photocatalyst. NO was chosen as the target pollutant with a typical indoor concentration in the first stage of this research since it is a typical inorganic pollutant in both indoor and outdoor conditions. The PCO experiments were performed under different indoor air conditions and results show that PCO is suitable for the indoor air quality improvement [1].

The modeling of the PCO has already been studied by some researchers so far. Hoffmann et al. [5] reviewed the reaction mechanism of the photocatalysis and especially the application of the Langmuir–Hinshelwood (L–H) model was studied. Obee and Brown [3] applied the L–H model to study the oxidation rate of some VOCs like formaldehyde, toluene, and 1,3-butadiene using an indoor air concentration of sub-ppm level and the effect of the humidity and pollutants concentration was considered in their model. They found that the effect of humidity on the oxidation rate is dependent critically on the concentration of the pollutant and the L–H model was successfully used to correlate the oxidation rate data. Dalton et al. [6] investigated the PCO of NO_x using TiO_2 as photocatalyst with a surface spectroscopic approach and the reaction mechanism. Devahasdin et al. [7] studied the reaction kinetics of NO photocatalytic oxidation and the effect of the space time and inlet pollutant concentration. Wang et al. [8] reported the reaction mechanism of PCO of NO_x with an inlet concentration of 20–168 ppm using TiO_2 sup-

* Corresponding author. Tel.: +31 040 247 2371; fax: +31 040 243 8595.
E-mail address: q.yu@bwk.tue.nl (Q.L. Yu).

0926-3373/$ – see front matter © 2010 Elsevier B.V. All rights reserved.
doi:10.1016/j.apcatb.2010.05.032

ported on a woven glass fabric, and they found that NO is oxidized to NO_2 both by the generated hydroxyl radicals and electron trapped oxygen. Kuo et al. [9] studied the PCO of NO_x under visible light using carbon-doped TiO_2 and they proposed a reaction mechanism in which NO is oxidized to NO_2 by the generated hydroxyl radicals and HO_2.

However, most of the studies on the photocatalytic reaction of NO are only focused on the way NO is oxidized to non-toxic product nitrates (NO_3^-) under outdoor air conditions. The modeling of the PCO of NO under indoor air conditions has not been reported before. As the influential parameters, the effect of the experimental conditions on the photocatalytic oxidation is rarely considered into the pollutant reaction rate [10]. Most researchers believe that NO is oxidized to NO_3^- via the intermediate product NO_2, however, the influence of this undesired intermediate product NO_2 is seldom investigated [11].

The present article addresses the PCO of NO under indoor air conditions and a kinetic model is proposed to describe this process. The reaction rate of the NO oxidation is derived from the PCO reaction mechanism of NO_x and the kinetic parameters are optimized using the experimental results presented in part I to this article [1]. In this model, the influence of the experimental conditions such as NO inlet concentration, volumetric flow rate of the NO, relative humidity, irradiance, dosage of the photocatalyst, and size of the reactor is incorporated, together as well as including the effect of the intermediate product NO_2. The proposed model is validated against the experimental data and the good agreement between the predicted values and the experimental results indicates its validity.

2. Experimental

The PCO test set-up used in this study for the indoor air quality assessment was developed using ISO standard 22197-1:2007 [12] as a reference, which focuses on advanced ceramics and advanced technical ceramics. The schematic diagram of the PCO set-up is shown in Fig. 1, which is composed of the reactor, visible light source, gas supply, and analyzer. The reactor is made of non-adsorbing plastic materials with a size of 100 mm × 200 mm ($W \times L$) allowing a planar sample to be embedded [13]. The applied light source consists of three cool day light lamps of each 25 W (Philips, The Netherlands), emitting a visible radiation in the range of 400–700 nm. The irradiance was measured using a VIS-BG radiometer (Dr. Gröbel UV-Elektronik GmbH, Germany). The used gas consists of 50 ppm NO stabilized in nitrogen (N_2), which then is diluted by a synthetic air to the desired concentration. The concentration of the pollutant (NO) and the intermediate product (NO_2) was analyzed using a chemiluminescent NO_x analyzer (HORIBA 370, Japan). A more detailed description of the experimental set-up is presented in [1].

Table 1
Experimental conditions.

Parameter	Standard conditions	Varying conditions
Reactor height, H (mm)	3	2–9
Initial NO concentration, $C_{NO,in}$ (ppm)	0.5	0.1–1.0
Volumetric flow rate, Q ($dm^3\ min^{-1}$)	3	1–5
Relative humidity, RH (%)	50	10–70
Irradiance, E ($W\ m^{-2}$)	10	1–13
Photocatalyst content, D_{TiO_2} ($g\ g^{-1}$)	0.5	0.02–0.5

The photocatalytic oxidation experiments were carried out using a standard procedure as introduced in [1]. The preparation of the PCO set-up according to the desired experimental conditions includes the warm-up of the NO_x analyzer, the preparation of the reactor, the flow of the gas to the system, and the parameters adjustment like irradiance, relative humidity, etc. The PCO test can be started once the experimental conditions are stable. The NO concentration decreases immediately when it flows through the reactor due to the feeding of the gas into the reactor and the adsorption of NO onto the surface of the sample, and then it increases again to the initial value within a short period of time which can be influenced by the factors like NO initial concentration, flow rate, and the surface structure of the tested sample. After this the photocatalytic oxidation reaction is started by allowing the visible light to irradiate the sample. The PCO reaction lasts 30 min in the present study and is ended by covering the reactor with an opaque material to cut off the irradiance.

Using ISO 22197-1:2007 [12] as a reference, a standard experimental condition was deployed in this study. An initial NO concentration was chosen as 500 ppb and the volumetric flow rate of NO as 3.0 L/min; the visible irradiance was chosen as 10 W/m^2 and a relative humidity of 50%. All the experiments were carried out at room temperature. The experimental conditions were varied to investigate their influence on the photocatalytic oxidation rate and the detailed information is shown in Table 1.

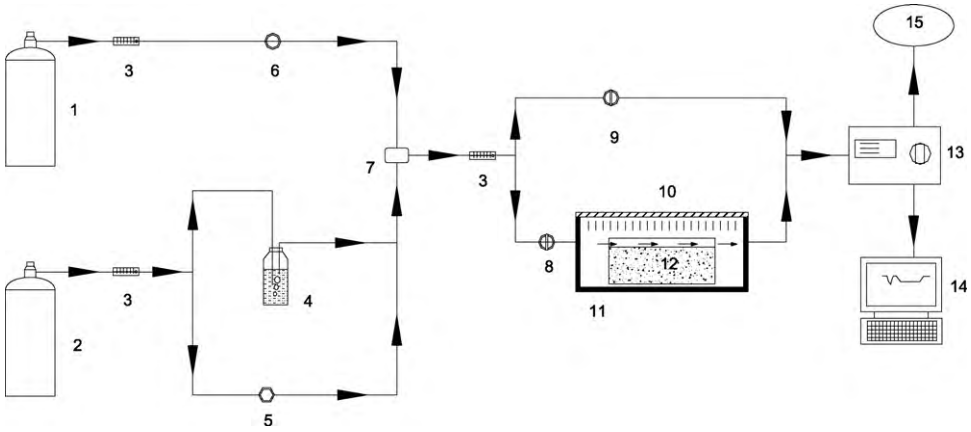

Fig. 1. Schematic diagram of photocatalytic degradation set-up. (1) NO gas supply, (2) synthetic air, (3) flow rate meter, (4) humidifier, (5) humidity controller, (6) NO concentration controller, (7) temperature and relative humidity sensor, (8) valve, (9) valve, (10) light source, (11) reaction chamber, (12) reactor, (13) NO_x analyzer, (14) computer and (15) vent.

3. Kinetic model

3.1. PCO mechanism of NO_x

As introduced in the previous section, once the experimental conditions become stable the pollutant (here NO) can be allowed to flow through the reactor. When the gas reactants are in contact with the photocatalyst, they are adsorbed onto the active sites over its surface. The process can be described by Eqs. (1)–(3), here TiO_2 represents the carbon modified TiO_2 used in the present study:

$$TiO_2 + H_2O \overset{K_{H_2O}}{\rightleftarrows} TiO_2\_H_2O \quad (1)$$

$$TiO_2 + O_2 \overset{K_{O_2}}{\rightleftarrows} TiO_2\_O_2 \quad (2)$$

$$TiO_2 + NO \overset{K_{NO}}{\rightleftarrows} TiO_2\_NO \quad (3)$$

The PCO process occurs at the surface of the photocatalyst by the reaction of NO with the hydroxyl radicals generated when the test sample is irradiated by the visible light. This process includes two steps of firstly the generation of electron/hole pairs and then the oxidation of NO.

Eqs. (4)–(6) describe the photon generation of electron/hole pairs and the trapping of the generated hole/electron pairs, respectively:

$$TiO_2 + h\nu \xrightarrow{\phi} e^- + h^+ \quad (4)$$

$$h^+ + TiO_2\_H_2O \xrightarrow{k_{h^+}} OH^\bullet + H^+ \quad (5)$$

$$e^- + TiO_2\_O_2 \xrightarrow{k_{e^-}} O_2^- \quad (6)$$

Eqs. (7)–(9) show the oxidation of NO by the hydroxyl radicals generated during the hole trapping to the final product NO_3^-:

$$TiO_2\_NO + OH^\bullet \xrightarrow{k_{NO}} TiO_2\_HNO_2 \quad (7)$$

$$TiO_2\_HNO_2 + OH^\bullet \xrightarrow{k_{HNO_2}} TiO_2\_NO_2 + H_2O \quad (8)$$

$$TiO_2\_NO_2 + OH^\bullet \xrightarrow{k_{NO_2}} NO_3^- + H^+ \quad (9)$$

As shown in Eqs. (7)–(9), the PCO of NO yields one final product, HNO_3, but two intermediate products are generated during the reaction. Devahasdin et al. [7] reported the reaction described in Eq. (7) occurs quickly at initial stage and the reaction described in Eq. (8) dominates the intermediate steps from NO to NO_3^-. Due to the desorption and mass transport of NO_2 from the surface of the sample to air (Eq. (10)), not all the produced NO_2 is consumed as reactant (Eq. (9)), which is confirmed in the previous study [1]:

$$TiO_2 + NO_2 \overset{K_{NO_2}}{\rightleftarrows} TiO_2\_NO_2 \quad (10)$$

During the PCO reaction, the generated electron/hole pairs can also be recombined again shown as Eq. (11). Evidently the recombination/deactivation of the electron/hole pairs decreases the activity of the applied photocatalyst:

$$e^+ + h^- \xrightarrow{k_{dea}} heat \quad (11)$$

3.2. Adsorption model

For the occurrence of PCO reaction, the first important step is the adsorption of the reactants onto the surface of the test sample (photocatalyst). The adsorption/desorption process reaches an equilibrium when the adsorption and desorption rate of a particular gas on the superficial active sites of photocatalyst [14] are equal:

$$r_+ - r_- = k_+ C_{TiO_2\_free} C_{GAS} - k_- C_{TiO_2\_GAS} = 0 \quad (12)$$

Thus,

$$C_{TiO_2\_GAS} = K_{GAS} C_{TiO_2\_free} C_{GAS} \quad (13)$$

where GAS denotes NO, NO_2, or H_2O, and $K_{GAS} = k_+/k_-$.

The total superficial concentration of active sites is composed of the concentration of the free sites and the occupied sites due to the adsorption of NO, NO_2 and H_2O:

$$C_{TiO_2} = C_{TiO_2\_free} + C_{TiO_2\_NO} + C_{TiO_2\_NO_2} + C_{TiO_2\_H_2O} \quad (14)$$

Here Eq. (14) is deduced based on the consideration that the adsorption of NO, NO_2, and H_2O does not compete with oxygen adsorption [15]. The reason lies in that O_2 is adsorbed in the conduction band of the photocatalyst, while other gases (here NO, NO_2 and H_2O) are trapped in the valence band of the photocatalyst [16].

Substituting the adsorbed gas concentration given by Eq. (13) in the case of NO, NO_2, and H_2O respectively into Eq. (14) gives:

$$C_{TiO_2} = C_{TiO_2\_free} + K_{NO} C_{TiO_2\_free} C_{NO} + K_{NO_2} C_{TiO_2\_free} C_{NO_2} + K_{H_2O} C_{TiO_2\_free} C_{H_2O} \quad (15)$$

Thus, $C_{TiO_2\_free}$ is obtained by rewriting Eq. (15), reads:

$$C_{TiO_2\_free} = \frac{C_{TiO_2}}{1 + K_{NO} C_{NO} + K_{NO_2} C_{NO_2} + K_{H_2O} C_{H_2O}} \quad (16)$$

Substituting the obtained expression for $C_{TiO_2\_free}$ (Eq. (16)) back into Eq. (13), the adsorption equilibrium concentration of all the gases are obtained respectively as follows:

$$C_{TiO_2\_NO} = \frac{K_{NO} C_{TiO_2} C_{NO}}{1 + K_{NO} C_{NO} + K_{NO_2} C_{NO_2} + K_{H_2O} C_{H_2O}} \quad (17)$$

$$C_{TiO_2\_NO_2} = \frac{K_{NO_2} C_{TiO_2} C_{NO_2}}{1 + K_{NO} C_{NO} + K_{NO_2} C_{NO_2} + K_{H_2O} C_{H_2O}} \quad (18)$$

$$C_{TiO_2\_H_2O} = \frac{K_{H_2O} C_{TiO_2} C_{H_2O}}{1 + K_{NO} C_{NO} + K_{NO_2} C_{NO_2} + K_{H_2O} C_{H_2O}} \quad (19)$$

The fundamental adsorption models derived here have the same format as the Langmuir adsorption isotherm, which has already been investigated to describe the adsorption of NO onto the surface of the photocatalyst for the PCO reaction [17]. In addition a reaction rate model, Langmuir–Hinshelwood model developed based on the Langmuir adsorption isotherm, has also been applied successfully to describe the reaction rate of PCO of NO [10,18].

As discussed above, O_2 here is trapped in the conduction band of the photocatalyst, therefore, the adsorption model of O_2 can be also obtained following the same procedure to deduce the adsorption model of the reactants that are adsorbed in the valence band of the photocatalyst:

$$C_{TiO_2'\_O_2} = \frac{K_{O_2} C_{TiO_2'} C_{O_2}}{1 + K_{O_2} C_{TiO_2'} C_{O_2}} \quad (20)$$

3.3. Reaction rate model

According to the mass action law and the fundamental reaction given in Eq. (7), the superficial reaction rate of NO is shown as follows:

$$r_{NO} = -k_{NO} C_{TiO_2\_NO} C_{OH^\bullet} \quad (21)$$

Since NO_2 is generated from HNO_2 and then is oxidized to NO_3^- as shown in Eqs. (8) and (9) respectively, the reaction rate of NO_2 reads:

$$r_{NO_2} = k_{HNO_2} C_{TiO_2\_HNO_2} C_{OH^\bullet} - k_{NO_2} C_{TiO_2\_NO_2} C_{OH^\bullet} \quad (22)$$

Assuming a microscopic local equilibrium for unstable intermediates, the superficial reaction rate for hydroxyl radicals reads:

$$r_{OH\bullet} = k_{h^+} C_{TiO_2\_H_2O} C_{h^+} - k_{NO} C_{TiO_2\_NO} C_{OH\bullet} - k_{HNO_2} C_{TiO_2\_HNO_2} C_{OH\bullet} - k_{NO_2} C_{TiO_2\_NO_2} C_{OH\bullet} = 0 \quad (23)$$

Therefore, $C_{OH\bullet}$ is obtained by rewriting Eq. (23), yielding:

$$C_{OH\bullet} = \frac{k_{h^+} C_{TiO_2\_H_2O} C_{h^+}}{k_{NO} C_{TiO_2\_NO} + k_{HNO_2} C_{TiO_2\_HNO_2} + k_{NO_2} C_{TiO_2\_NO_2}} \quad (24)$$

With the hypothesis that, as an intermediate, HNO_2 is produced and very rapidly consumed, $C_{TiO_2\_HNO_2}$ is therefore obtained as follows:

$$r_{HNO_2} = k_{NO} C_{TiO_2\_NO} C_{OH\bullet} - k_{HNO_2} C_{TiO_2\_HNO_2} C_{OH\bullet} = 0 \quad (25)$$

$$C_{TiO_2\_HNO_2} = \frac{k_{NO} C_{TiO_2\_NO}}{k_{HNO_2}} \quad (26)$$

The reaction rates of the generated electron/hole pairs are expressed as follows:

$$r_{e^-} = r_{act} - k^*_{e^-} C_{e^-} - k_{dea} C_{e^-} C_{h^+} = 0 \quad (27)$$

$$r_{h^+} = r_{act} - k_{h^+} C_{TiO_2\_H_2O} C_{h^+} - k_{dea} C_{e^-} C_{h^+} = 0 \quad (28)$$

Where $k^*_{e^-} = k_{e^-} C_{TiO'_2\_O_2} = k_{e^-}((K_{O_2} C_{TiO'_2} C_{O_2})/(1 + K_{O_2} C_{TiO'_2} C_{O_2}))$ assuming that $C_{TiO'_2\_O_2}$ is constant since O_2 in the air is in huge excess compared to the concentration of the pollutant.

The reaction rate of the photocatalyst activation (r_{act}) along the thickness (t) of the photocatalyst layer and under all wavelengths in the range of the lamps emission that the photocatalyst absorbs can be expressed as a function of the local superficial rate of photon absorption $e^a_{S,\lambda}$ and the primary quantum yield ϕ_λ [19,20], reads:

$$r_{act} = \int_{y=0}^{y=t} \int_\lambda \phi_\lambda e^a_{S,\lambda}(y)\, d\lambda\, dy = \int_{y=0}^{y=t} \int_\lambda \phi_\lambda S_g \rho D_{TiO_2} \kappa_\lambda E_\lambda(y)\, d\lambda\, dy \quad (29)$$

Assuming an absorbent medium, the radiation extinction along the thickness of the photocatalyst layer can be expressed according to Beer–Lambert law as follows:

$$E_\lambda(y) = E_\lambda e^{-\kappa_\lambda y} \quad (30)$$

Therefore, integrating along the thickness of the photocatalyst and assuming that every property is constant in the uniform thickness, Eq. (29) is rewritten as:

$$r_{act} = \int_{y=0}^{y=t} \int_\lambda \phi_\lambda S_g \rho D_{TiO_2} \kappa_\lambda E_\lambda e^{-\kappa_\lambda y}\, d\lambda\, dy = E \int_\lambda \phi_\lambda S_g \rho D_{TiO_2} (1 - e^{-\kappa_\lambda t})\, d\lambda = \alpha E \quad (31)$$

where

$$\alpha = \int_\lambda \phi_\lambda S_g \rho D_{TiO_2} (1 - e^{-\kappa_\lambda t})\, d\lambda \quad (32)$$

Therefore, C_{h^+} and C_{e^-} are obtained from Eqs. (27), (28) and (31):

$$C_{e^-} = \frac{\alpha E}{k^*_{e^-} + k_{dea} C_{h^+}} \quad (33)$$

$$C_{h^+} = \frac{\alpha E}{k_{h^+} C_{TiO_2\_H_2O} + k_{dea} C_{e^-}} = \frac{\alpha E}{k_{h^+} C_{TiO_2\_H_2O} + k_{dea}((\alpha E)/(k^*_{e^-} + k_{dea} C_{h^+}))} \quad (34)$$

C_{h^+} can be solved from Eq. (34) and the positive sign of the quadratic solution is chosen since C_{h^+} is 0 if E is 0, yielding:

$$C_{h^+} = \frac{k^*_{e^-}\left(\sqrt{((1 + (4k_{dea}\alpha E)/(k^*_{e^-} k_{h^+} C_{TiO_2\_H_2O}))} - 1\right)}{2k_{dea}} \quad (35)$$

Substituting the obtained C_{h^+} from Eq. (35) and Eq. (26) into Eq. (24), $C_{OH\bullet}$ is obtained:

$$C_{OH\bullet} = \frac{k^*_{e^-} k_{h^+} C_{TiO_2\_H_2O}\left(\sqrt{1 + ((4k_{dea}\alpha E)/(k^*_{e^-} k_{h^+} C_{TiO_2\_H_2O}))} - 1\right)}{4k_{dea} k_{NO} C_{TiO_2\_NO} + 2k_{dea} k_{NO_2} C_{TiO_2\_NO_2}} \quad (36)$$

Substituting the obtained $C_{OH\bullet}$ into Eqs. (21) and (22), the reaction rate model for NO and NO_2 now is derived as:

$$r_{NO} = \frac{-k_{NO} C_{TiO_2\_NO} \gamma C_{TiO_2\_H_2O}}{4k_{NO} C_{TiO_2\_NO} + 2k_{NO_2} C_{TiO_2\_NO_2}} \left(\sqrt{1 + \frac{4\alpha E}{\gamma C_{TiO_2\_H_2O}}} - 1\right) \quad (37)$$

and

$$r_{NO_2} = \frac{(k_{NO} C_{TiO_2\_NO} - k_{NO_2} C_{TiO_2\_NO_2}) \gamma C_{TiO_2\_H_2O}}{4k_{NO} C_{TiO_2\_NO} + 2k_{NO_2} C_{TiO_2\_NO_2}} \left(\sqrt{1 + \frac{4\alpha E}{\gamma C_{TiO_2\_H_2O}}} - 1\right) \quad (38)$$

respectively, where

$$\gamma = \frac{k_{h^+} \times k^*_{e^-}}{k_{dea}} \quad (39)$$

3.4. Mass balance

The following aspects are usually considered in reactor design [21]: raw materials, operating conditions, geometry of the reactor, radiation source, etc. Different types of reactors can be used for photocatalytic reactions [22,23], among them three types of reactors are usually considered as ideal reactors [24], which are batch reactor, plug flow reactor, and continuously mixed reactor.

In a plug flow reactor, the fluid flows along the reactor orderly with no element overtaking or mixing with any other element ahead or behind. All reactants in the plug flow reactor have the same residence time [25]. The reactor used in the present study can be assumed as a plug flow reactor according to the description above and the analyses from [11,26]. For this kind of reactor configuration, NO and NO_2 are consumed or generated along the reactor as follows:

$$v_{air} \frac{dC_{NO}}{dx} = a_v r_{NO} \quad (40)$$

$$v_{air} \frac{dC_{NO_2}}{dx} = a_v r_{NO_2} \quad (41)$$

With the following boundary conditions:

$$C_{NO}(x = 0) = C_{NO,in} \quad (42)$$

$$C_{NO_2}(x = 0) = C_{NO_2,in} \quad (43)$$

Here a_v, the active surface area per unit of reactor volume related with the dosage of the photocatalyst, is applied in the mass balances given by Eqs. (40) and (41) since the PCO reaction only occurs on the surface of the sample (photocatalyst) and reads:

$$a_v = \frac{D_{TiO_2} A_{reactor}}{V_{reactor}} \cong \frac{D_{TiO_2}}{H} \quad (44)$$

The concentration of NO and NO_2 along the reactor is solved numerically applying the Euler method after substituting Eqs. (37)

and (38) into Eqs. (40) and (41) respectively, yielding:

$$v_{air}\frac{C_{NO,i+1}-C_{NO,i}}{x_{i+1}-x_i} = \frac{-a_v\gamma k_{NO}C_{TiO_2\_NO,i}C_{TiO_2\_H_2O}}{(4k_{NO}C_{TiO_2\_NO,i}+2k_{NO_2}C_{TiO_2\_NO_2,i})}\left(\sqrt{1+\frac{4\alpha E}{\gamma C_{TiO_2\_H_2O}}}-1\right) \quad (45)$$

$$v_{air}\frac{C_{NO_2,i+1}-C_{NO_2,i}}{x_{i+1}-x_i} = \frac{a_v\gamma(k_{NO}C_{TiO_2\_NO,i}-k_{NO_2}C_{TiO_2\_NO_2,i})C_{TiO_2\_H_2O}}{(4k_{NO}C_{TiO_2\_NO,i}+2k_{NO_2}C_{TiO_2\_NO_2,i})} \times\left(\sqrt{1+\frac{4\alpha E}{\gamma C_{TiO_2\_H_2O}}}-1\right) \quad (46)$$

where $i = 1, 2, \ldots, n$, and $x_{i+1} - x_i = L/(n-1)$.

Therefore, the concentration of NO and NO_2 along the reactor is obtained as follows:

$$C_{NO,i+1} = \frac{(x_{i+1}-x_i)}{v_{air}}\frac{-a_v\gamma k_{NO}C_{TiO_2\_NO,i}C_{TiO_2\_H_2O}}{(4k_{NO}C_{TiO_2\_NO,i}+2k_{NO_2}C_{TiO_2\_NO_2,i})} \times\left(\sqrt{1+\frac{4\alpha E}{\gamma C_{TiO_2\_H_2O}}}-1\right)+C_{NO,i} \quad (47)$$

$$C_{NO_2,i+1} = \frac{x_{i+1}-x_i}{v_{air}}\frac{a_v\gamma(k_{NO}C_{TiO_2\_NO,i}-k_{NO_2}C_{TiO_2\_NO_2,i})C_{TiO_2\_H_2O}}{(4k_{NO}C_{TiO_2\_NO,i}+2k_{NO_2}C_{TiO_2\_NO_2,i})} \times\left(\sqrt{1+\frac{4\alpha E}{\gamma C_{TiO_2\_H_2O}}}-1\right)+C_{NO_2,i} \quad (48)$$

4. Results and discussion

4.1. Results

The concentration of NO and NO_2 in Eqs. (47) and (48) is described using the superficial adsorbed concentration of reactants (NO, NO_2, and H_2O), and they can be expressed as the volumetric concentration in air by substituting Eqs. (17)–(19) to Eqs. (47) and (48), respectively. Therefore, a full model of the concentration of NO and NO_2 along the reactor during the PCO reaction is obtained:

$$C_{NO,i+1} = \frac{x_{i+1}-x_i}{v_{air}}\frac{-a_v k_{NO}\beta K_{NO}K_{H_2O}C_{NO,i}C_{H_2O}\left(\sqrt{(1+(4\alpha E(1+K_{NO}C_{NO,i}+K_{NO_2}C_{NO_2,i}+K_{H_2O}C_{H_2O}))/(\beta K_{H_2O}C_{H_2O})}-1\right)}{(4k_{NO}K_{NO}C_{NO,i}+2k_{NO_2}K_{NO_2}C_{NO_2,i})(1+K_{NO}C_{NO,i}+K_{NO_2}C_{NO_2,i}+K_{H_2O}C_{H_2O})}+C_{NO,i} \quad (49)$$

$$C_{NO_2,i+1} = \frac{x_{i+1}-x_i}{v_{air}}\frac{a_v\beta(k_{NO}K_{NO}C_{NO,i}-k_{NO_2}K_{NO_2}C_{NO_2,i})K_{H_2O}C_{H_2O}}{(4k_{NO}K_{NO}C_{NO,i}+2k_{NO_2}K_{NO_2}C_{NO_2,i})(1+K_{NO}C_{NO,i}+K_{NO_2}C_{NO_2,i}+K_{H_2O}C_{H_2O})} \times\left(\sqrt{1+\frac{4\alpha E(1+K_{NO}C_{NO,i}+K_{NO_2}C_{NO_2,i}+K_{H_2O}C_{H_2O})}{\beta K_{H_2O}C_{H_2O}}}-1\right)+C_{NO_2,i} \quad (50)$$

where

$$\beta = \frac{k_{h^+}\times k^*_{e^-}}{k_{dea}}\times C_{TiO_2} \quad (51)$$

The kinetic parameters in Eqs. (49) and (50) then are obtained by optimizing these two equations employing the "Solver" tool from Microsoft Excel and the experimental data [1]. The results are listed in Table 2.

Since in the present study, the concentration of NO, NO_2, and H_2O is in the order of 10^{-8}, 10^{-9}, and 10^{-4}, respectively, then for the optimized value of K_{NO}, K_{NO_2}, and K_{H_2O} the denominator of Eqs. (17)–(19) can be equaled to unity without causing significant error. Therefore the complete model (Eqs. (49) and (50)) can be simplified according to this, yielding:

$$C_{NO,i+1} = a_v\frac{(x_{i+1}-x_i)}{v_{air}}\frac{-k'_{NO}\beta' C_{NO,i}C_{H_2O}}{(4k'_{NO}C_{NO,i}+2k'_{NO_2}C_{NO_2,i})} \times\left(\sqrt{1+\frac{4\alpha E}{\beta' C_{H_2O}}}-1\right)+C_{NO,i} \quad (52)$$

$$C_{NO_2,i+1} = a_v\frac{x_{i+1}-x_i}{v_{air}}\frac{\beta'(k'_{NO}C_{NO,i}-k'_{NO_2}C_{NO_2,i})C_{H_2O}}{(4k'_{NO}C_{NO,i}+2k'_{NO_2}C_{NO_2,i})} \times(\sqrt{1+((4\alpha E)/(\beta' C_{H_2O}))}-1)+C_{NO_2,i} \quad (53)$$

where

$$k'_{NO} = k_{NO}K_{NO},\ k'_{NO_2} = k_{NO_2}K_{NO_2} \text{ and } \beta' = \beta K_{H_2O} \quad (54)$$

The parameters in Eqs. (52) and (53) then are again obtained using optimization employing the experimental results from the previous study [1]. The results are listed in Table 3.

Fig. 2 shows the outlet concentration of NO and NO_2 predicted by the simplified model versus the concentration of NO and NO_2 obtained from the experiments [1]. It shows clearly a good agreement between the model predictions and experimental results, which indicates evidently the validity of the proposed kinetic model.

From Eqs. (40) and (41), a relation between the outlet concentration of NO and NO_2 is obtained, reading:

$$\frac{dC_{NO}}{dC_{NO_2}} = \frac{-k_{NO}K_{NO}C_{NO}}{k_{NO}K_{NO}C_{NO}-k_{NO_2}K_{NO_2}C_{NO_2}} = \frac{-k'_{NO}C_{NO}}{k'_{NO}C_{NO}-k'_{NO_2}C_{NO_2}} \quad (55)$$

with the following boundary condition:

$$C_{NO_2}(C_{NO} = C_{NO,in}) = 0 \quad (56)$$

Table 2
Parameters optimized from the full model.

Parameter	Value
k_{NO} ($dm^2\ mol^{-1}\ min^{-1}$)	3.21×10^{-9}
k_{NO_2} ($dm^2\ mol^{-1}\ min^{-1}$)	1.19×10^{-7}
K_{NO} ($dm^3\ mol^{-1}$)	2.09×10^{4}
K_{NO_2} ($dm^3\ mol^{-1}$)	5.38×10^{3}
K_{H_2O} ($dm^3\ mol^{-1}$)	2.39×10^{0}
α ($mol\ W^{-1}\ min^{-1}$)	4.32×10^{-2}
β ($mol\ dm^{-2}\ min^{-1}$)	6.20×10^{-8}

Table 3
Parameters optimized from the simplified model.

Parameter	Value
k'_{NO} ($dm^5\ mol^{-2}\ min^{-1}$)	4.50×10^{-5}
k'_{NO_2} ($dm^5\ mol^{-2}\ min^{-1}$)	5.02×10^{-4}
α ($mol\ W^{-1}\ min^{-1}$)	3.72×10^{-2}
β' ($dm\ min^{-1}$)	2.49×10^{-7}

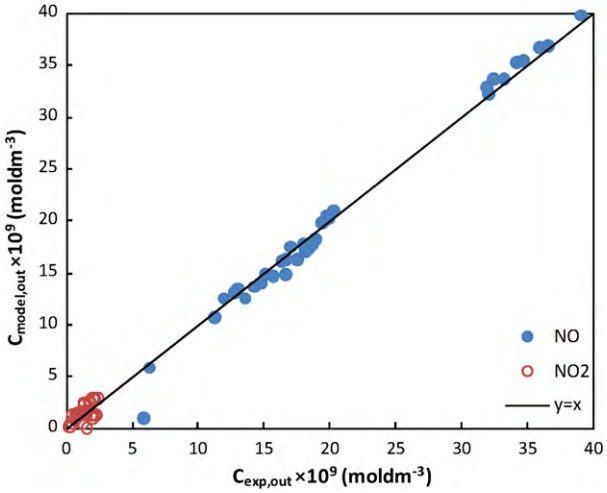

Fig. 2. Predictions of the NO and NO_2 outlet concentration from the models versus the experimental results.

Eq. (55) is solved analytically employing the boundary condition (Eq. (56)), yielding:

$$C_{NO_2} = \frac{C_{NO}}{k'_{NO_2}k'_{NO} - 1} - \frac{C_{NO,in}}{k'_{NO_2}/k'_{NO} - 1}\left(\frac{C_{NO}}{C_{NO,in}}\right)^{k'_{NO_2}/k'_{NO}} \quad (57)$$

Eq. (57) can be simplified since $C_{NO} < C_{NO,in}$ and $k'_{NO_2}/k'_{NO} = 11.2$ by taking the values of k'_{NO} and k'_{NO_2} from Table 3, hence a linear relation between the outlet concentration of NO and NO_2 is derived, reading:

$$C_{NO} = 10.2C_{NO_2} \quad (58)$$

The outlet concentration of NO and NO_2 obtained from experiments [1] are plotted shown as Fig. 3. It is shown from Fig. 3 that the average value of the proportion of the concentration of NO and NO_2 is 11.7, which is in line with the derived results here. This also confirms the validity of the proposed model.

4.2. Discussion

As presented in part I to this article [1] and also in [27,28], experimental conditions influence significantly the photocatalytic degradation performance. Therefore, in order to develop a representative model, the incorporation of the experimental conditions is of vital importance. From the developed model (Eqs. (52) and (53)) one can see that all the experimental conditions such as initial pollutant (NO) concentration, volumetric flow rate, relative humidity, irradiance, reactor size, and dosage of the photocatalyst are represented. Figs. 4–9 show the predicted results from the proposed model versus the experimental results under different experimental conditions. It should be mentioned that all other

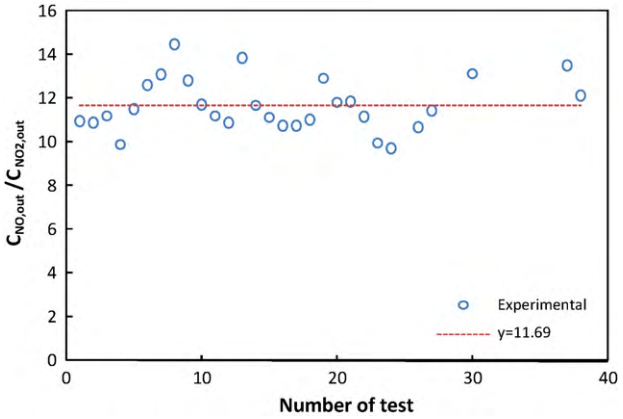

Fig. 3. The relation between outlet concentration of NO and NO_2.

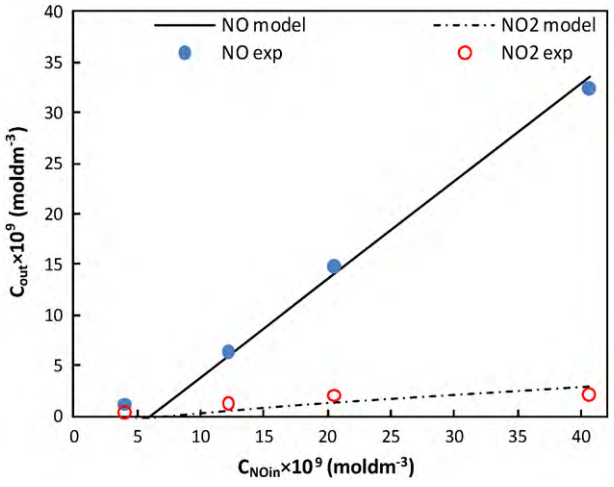

Fig. 4. Model predictions versus the experimental results (effect of the initial NO concentration).

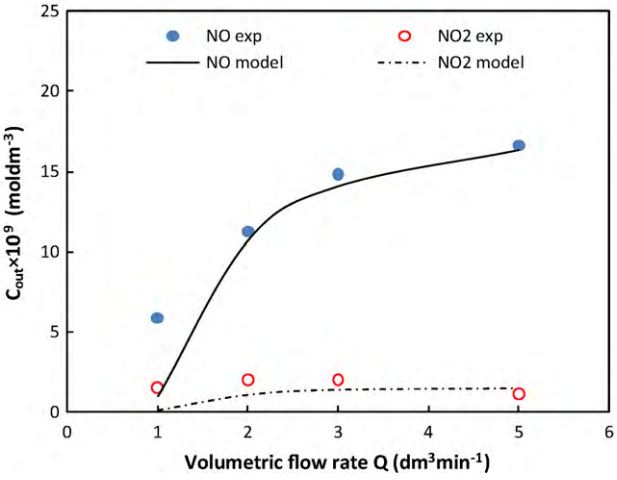

Fig. 5. Model predictions versus the experimental results (effect of the flow rate).

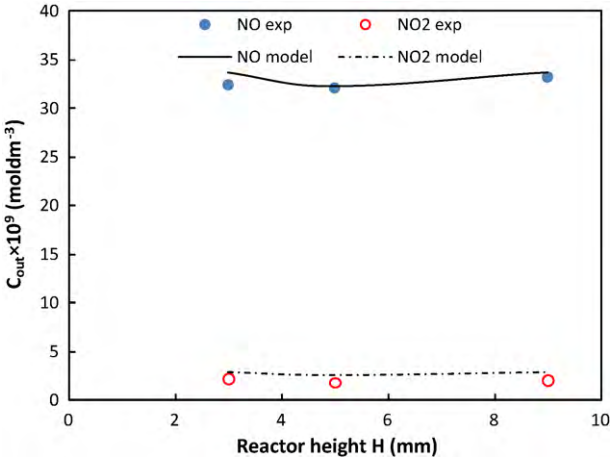

Fig. 6. Model predictions versus the experimental results (effect of the reactor size).

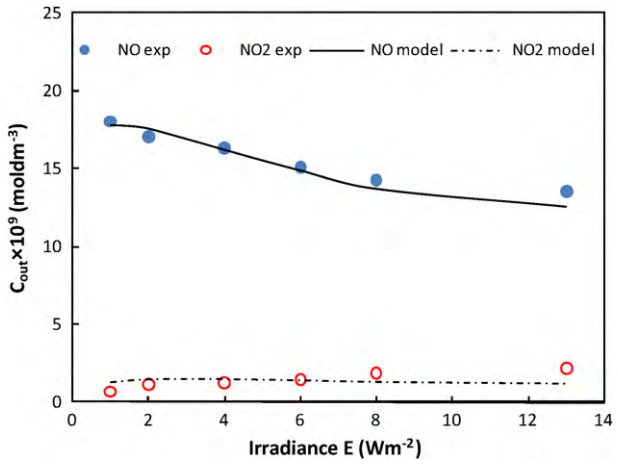

Fig. 7. Model predictions versus the experimental results (effect of the irradiance).

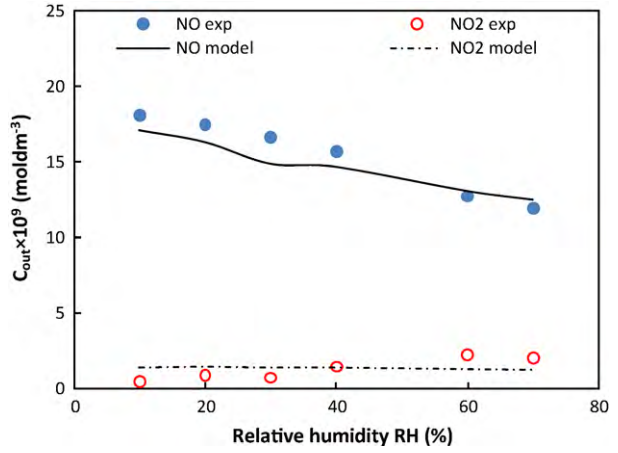

Fig. 8. Model predictions versus the experimental results (effect of the relative humidity).

experimental conditions remain standard as presented in Section 2 when one parameter is changed. It is evident from Figs. 4–9 that the proposed model provides correct predictions even under different experimental conditions. This shows clearly that this new developed model can be applied validly in conditions described in the present study.

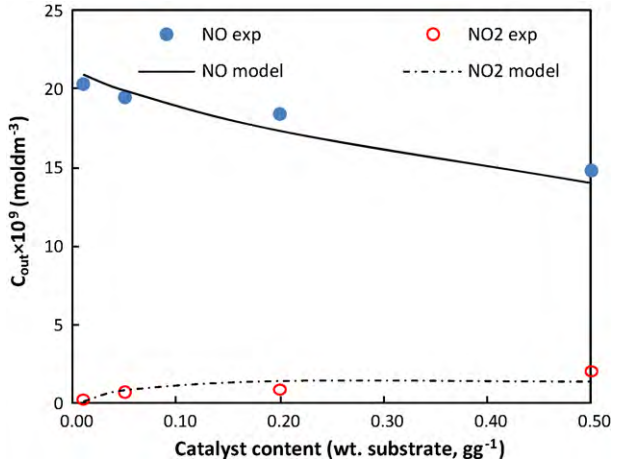

Fig. 9. Model predictions versus the experimental results (effect of the photocatalyst dosage).

As described in Section 3.1, NO_2 is generated during the PCO of NO and it could not be oxidized completely in this process [1], and actually NO_2 is even more toxic than NO. Therefore, the proposed model incorporates NO_2 from its reaction mechanism, adsorption isotherm and reaction rate as well. The prediction values versus the measured experimental results of NO_2 presented in Figs. 4–9 indicates the validity of the proposed model. The linear relation between the outlet concentration of NO and NO_2 derived here is confirmed by Ballari et al. [11], who investigated the PCO of NO with the traditional TiO_2 as photocatalyst applying pavestone as substrate for the outdoor air purification research and found a linear relation of 11.0–11.9 between the outlet concentration of NO and NO_2. The comparable results also support the validity of the new proposed model.

Nevertheless, regarding the validity of the proposed models, they hold only for the present experimental conditions, i.e. a strict lab scale test conditions, as shown in Table 1. To investigate the behavior of the PCO under real indoor air conditions, a reactor with a size of 200 L is developed, which will also be applied to validate the new proposed kinetic model in the near future. Later on also a real scale demonstration room will be built to investigate the PCO behavior under indoor air conditions, and the present proposed model will be applied to this set-up as well.

5. Conclusion

This article addresses the kinetics of the heterogeneous photocatalytic oxidation (PCO) for the indoor air purification employing nitric oxide as target pollutant. A kinetic model is proposed to describe the photocatalytic degradation of NO under indoor experimental conditions. This new proposed model incorporates the influences of experimental conditions such as initial pollutant concentration, volumetric flow rate of the pollutant, relative humidity, irradiance, dosage of the photocatalyst, and reactor size since they affect significantly the PCO behavior. As an undesired intermediate product, NO_2 influences the degradation rate of NO by affecting the adsorption and oxidation process, which is also considered into this new model. Applying the experimental results from the first part to this study [1], the parameters presented in the proposed model are optimized. The good agreement between the predictions from the model and experimental results indicates the validity of the model. Therefore, the new proposed model can be applied to describe the behavior of the photocatalytic degradation of NO under indoor air conditions.

Nevertheless, as discussed above, this model is proposed based on a certain conditions described in this article, hence, to extend it to be used effectively into other conditions, further investigation is still very necessary. Furthermore, this model is proposed to describe the behavior of NO degradation under indoor air conditions, however, there are also organic pollutants in indoor buildings such as volatile organic compounds (VOCs) which also are harmful to the health of human beings. Thus to develop a suitable model to describe the behavior of the degradation of organic pollutants under indoor conditions, especially to interpret the difference of the PCO behavior of organic and inorganic pollutants degradation is also of vital importance. The present results will be used as a basis for the further research in indoor air quality improvement.

List of symbols

Roman

A	area (mm^2)
a_v	the active surface area per unit of reactor volume (dm^{-1})
C	concentration (mol dm^{-3})
C_{TiO_2}	superficial concentration in valance band (mol dm^{-2})

$C_{TiO_2'}$	superficial concentration in conduction band (mol dm^{-2})
D_{TiO_2}	dosage of the photocatalyst (g g^{-1})
E	irradiance on the surface of photocatalyst (W m^{-2})
e^-	electron
h^+	electron hole
H	height of the reactor (mm)
k	reaction rate constant (dm^2 mol^{-1} min^{-1})
k^*	a group of parameters of k and C_{TiO_2} (min^{-1})
k'	a group of parameters of k and K (dm^5 mol^{-2} min^{-1})
K	adsorption constant (dm^3 mol)
L	length of the reactor (mm)
r	reaction rate (mol dm^{-2} min^{-1})
RH	relative humidity
Q	volumetric flow rate (dm^3 min^{-1})
S_g	specific surface area (dm^2 g^{-1})
t	thickness of the photocatalyst layer (dm)
V	volume of the reactor (dm^3)
v	linear velocity (dm min^{-1})
W	width of the reactor (mm)

Greek

α	parameter, irradiance related (mol W^{-1} min^{-1})
β	a group of parameters of γ and sites (mol dm^2 min^{-1})
β'	a group of parameters of β and adsorption constant of water (dm min^{-1})
κ	radiation absorption coefficient of the photocatalyst (cm^{-1})
ϕ	primary quantum yield (mol W^{-1} min^{-1})
λ	wavelength of the applied light source (nm)
ρ	density of the photocatalyst (g dm^{-3})
γ	a group of parameters of k_{h^+}, $k^*_{e^-}$, and k_{dea} (min^{-1})

Subscripts

act	activation
ads	adsorption
air	air
dea	deactivation
e^-	electron
exp	experimental
GAS	gas
h^+	electron hole
H_2O	water
HNO_2	HNO_2
in	inlet concentration
λ	wavelength of the applied light source (nm)
model	model
NO	nitric oxide
NO_2	nitrogen dioxide
$OH^\bullet$	hydroxyl radicals
reactor	reactor
out	outlet concentration

Acknowledgements

The authors wish to express their gratitude to the European Commission (I-SSB Project, Proposal No. 026661-2) for funding this research and the following sponsors of the research group: Bouwdienst Rijkswaterstaat, Graniet-Import Benelux, Kijlstra Betonmortel, Insulinde, Eerland Recycling, ENCI, Provincie Overijssel, Rijkswaterstaat Directie Zeeland, A&G Maasvlakte, BTE, Alvon Bouwsystemen, v.d. Bosch Beton, and Twee "R" Recycling, and GMB (chronological order of joining), and thanks are also expressed to P. Spiesz M.Sc. for his contribution to this article.

References

[1] Q.L. Yu, H.J.H. Brouwers, Appl. Catal. B: Environ. 92 (2009) 454–461.
[2] M. Hunger, H.J.H. Brouwers, Proceedings of the International Conference on Microstructure Related Durability of Cementitious Composites, Nanjing, China, October 2008, pp. 1103–1112.
[3] T.N. Obee, R.T. Brown, Environ. Sci. Technol. 29 (1995) 1223–1231.
[4] EU Project, The Integrated Safe & Smart Built Concept (I-SSB), URL: http://www.issb-project.com/.
[5] M.R. Hoffmann, S.T. Martin, W. Choi, D.W. Bahnemann, Chem. Rev. 95 (1995) 69–96.
[6] J.S. Dalton, P.A. Janes, N.G. Jones, J.A. Nicholson, K.R. Hallam, G.C. Allen, Environ. Pollut. 120 (2002) 415–422.
[7] S. Devahasdin, C. Fan, J.K. Li, D.H. Chen, J. Photochem. Photobiol. A: Chem. 156 (2003) 161–170.
[8] H. Wang, Z. Wu, W. Zhao, B. Guan, Chemosphere 66 (2007) 185–190.
[9] C.S. Kuo, Y.H. Tseng, C. Huang, Y. Li, J. Mol. Catal. A: Chem. 270 (2007) 93–100.
[10] M. Hunger, G. Hüsken, H.J.H. Brouwers, Cement Concrete Res. 40 (2010) 313–320.
[11] M.M. Ballari, M. Hunger, G. Hüsken, H.J.H. Brouwers, Appl. Catal. B: Environ 95 (2010) 245–254.
[12] International Organization for Standardization, ISO 22197-1:2007, Switzerland.
[13] G. Hüsken, M. Hunger, H.J.H. Brouwers, Proceedings of the International RILEM Symposium on Photocatalysis, Environment and Construction Materials—TDP, RILEM Publications, Bagneux, France, October 2007, pp. 147–154.
[14] M.M. Ballari, O.M. Alfano, A.E. Cassano, Ind. Eng. Chem. Res. 48 (2009) 1847–1858.
[15] C.S. Turchi, D.F. Ollis, J. Catal. 122 (1990) 178–192.
[16] S.P. Blößl, L. Elfenthal, Proceedings of the International RILEM Symposium on Photocatalysis, Environment and Construction Materials—TDP, RILEM Publications, Bagneux, France, October 2007, pp. 31–38.
[17] K. Hashimoto, K. Wasada, M. Osaki, E. Shono, K. Adachi, N. Toukai, H. Kominami, Y. Kera, Appl. Catal. B: Environ. 20 (2001) 429–436.
[18] Q.L. Yu, M.M. Ballari, H.J.H. Brouwers, Proceedings of the 3rd International Symposium on Nanotechnology in Construction, Springer-Verlag, Berlin, Heidelberg, June 2009, pp. 389–394.
[19] G.E. Imoberdorf, H.A. Irazoqui, A.E. Cassano, O.M. Alfano, Ind. Eng. Chem. Res. 44 (2005) 6075–6085.
[20] G.E. Imoberdorf, A.E. Cassano, O.M. Alfano, H.A. Irazoqui, AIChE 52 (2006) 1814–1823.
[21] A.E. Cassano, C.A. Martin, R.J. Brandi, O.M. Alfano, Ind. Eng. Chem. Res. 34 (1995) 2155–2201.
[22] A.E. Cassano, O.M. Alfano, Catal. Today 58 (2000) 167–197.
[23] H. de Lasa, B. Serrano, M. Salaices, Photocatalytic Reaction Engineering, Springer, 2005.
[24] O. Levenspiel, Chemical Reaction Engineering, Willey, New York, 1999.
[25] J. Zhao, X.D. Yang, Build. Environ. 38 (2003) 645–654.
[26] M. Hunger, H.J.H. Brouwers, M.M. Ballari, Proceedings of the International Conference on Microstructure related Durability of Cementitious Composites, Nanjing, China, October 2008, pp. 1103–1112.
[27] G. Hüsken, M. Hunger, H.J.H. Brouwers, Build. Environ. 44 (2009) 2463–2474.
[28] A. Beeldens, Proceedings of the International RILEM Symposium on Photocatalysis, Environment and Construction Materials—TDP, RILEM Publications, Bagneux, France, October 2007, pp. 187–194.